

Cyclic Aromatic 6π -Electron S_2N_2 - A Ligand with Tunable σ - and π - Donor-Acceptor Property

Susmita De¹ and Mohammed Sadik¹

¹Cochin University of Science and Technology

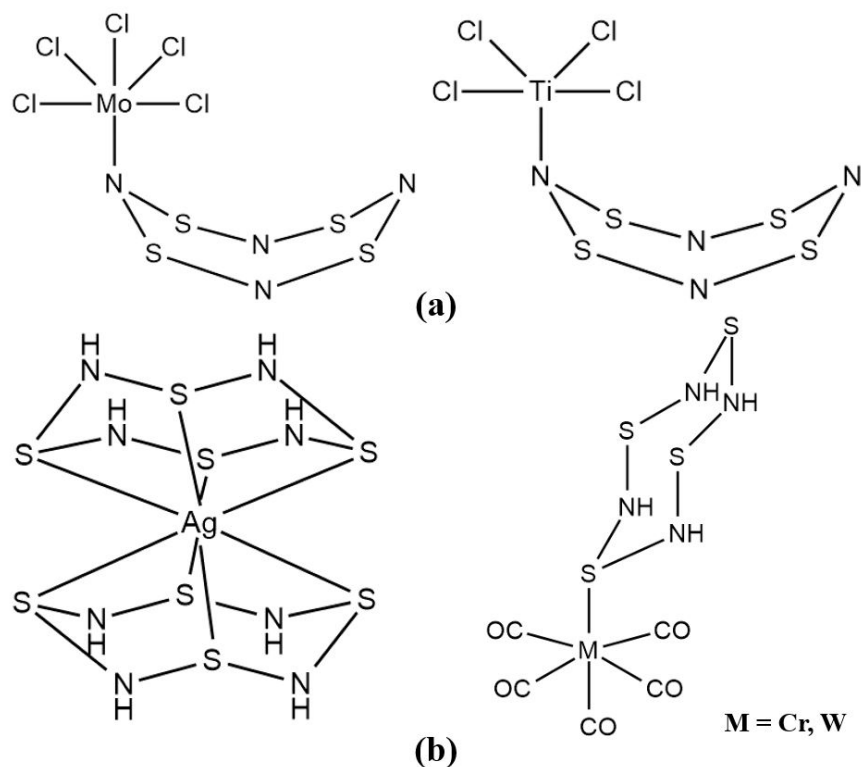
August 22, 2020

Abstract

The usage of inorganic aromatic N-donor based ligands, whose electronic properties can be easily and extensively tuned, are still underdeveloped. One such system is cyclic compounds of sulfur-nitrogen, which is known to form η^1 and η^2 -complexes with mono- and bi-metallic transition metal fragments. We have undertaken an extensive theoretical investigation of the bonding nature between S_2N_2 ligand and 14 valence electron (VE) metal fragments in the mono and bi-metallic $S_2N_2[Mo(NO)Cl_4]^-$ and $S_2N_2[Mo_2(NO)_2(Cl)_8]^{2-}$. Our results indicate that S_2N_2 ligand in $S_2N_2[Mo(NO)Cl_4]^-$ is a σ -donor and π -acceptor. The EDA-NOCV analysis indicates that the interaction between S_2N_2 and metal fragments has a higher electrostatic character than a covalent character. The nature of S_2N_2 as a ligand is similar in the bi-metallic complex $S_2N_2[Mo_2(NO)_2(Cl)_8]^{2-}$ as well. On the contrary, the σ -lone pair on N-atom in S_2N_2 is donated to the electron-deficient 12 valence electron $[Mo(NO)Cl_4]^+$ fragment in $S_2N_2[Mo(NO)Cl_4]^+$ and the electrons from the S_2N_2 π -MO are donated to the vacant d-orbitals of the metal fragment. Similar bonding nature is also observed in the bi-metallic $S_2N_2[Mo_2(NO)_2(Cl)_8]^{2+}$ complex. Besides, all these complexes show donation of lone pair on Cl attached to transition metal fragment to the S-N σ^* -MO, which is majorly located on the S-atom. Here, the S-atom in S_2N_2 can be considered as a σ -hole, which is involved in the chalcogen bond formation by accepting an electron pair from Cl-atom. Hence, our theoretical calculations suggest that the S_2N_2 is a versatile ligand which can be tuned as σ -donor, σ - acceptor, π -donor and π -acceptor.

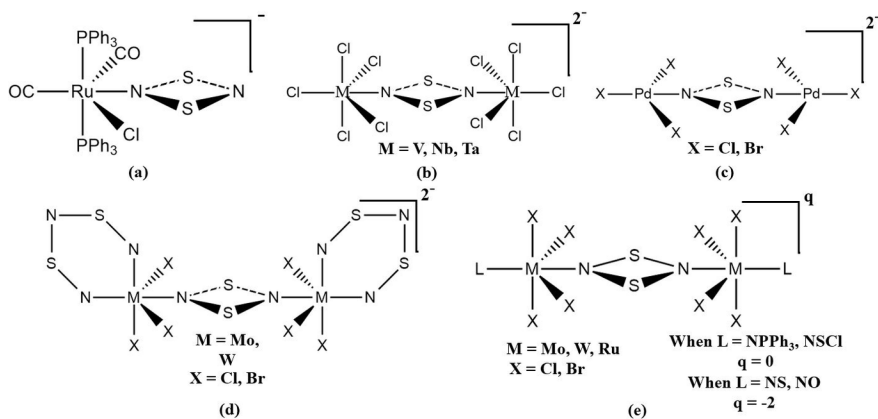
Introduction

N-donor aromatic hydrocarbons, such as pyridine and its structural analogs represent a class of extremely valued ligands and ubiquitously have played important roles in the development of coordination chemistry.^[1-6] Interestingly, the heteroatom substitution in the aromatic hydrocarbons introduces Lewis basicity due to σ -lone pair of nitrogen and Lewis acidity due to C-N π^* -orbitals.^[6-9] Moreover, the interactions of these classes of compounds with the transition metal fragments could be widely varied from the formation of σ -type or π -type complexes. Accordingly, a wide variety of N-based aromatic hydrocarbon ligands has been designed and synthesized in order to generate organometallic compounds with diverse structures, shapes, nuclearity and dimensionality.^[3,6,10,11] The diversity in the chemistry of such ligands have been heavily utilized for different applications in the field of biomedical applications, thermal reaction batteries, semiconducting materials and catalysis.^[12-16]



Scheme 1: Schematic representation of (a) MoCl₅.S₄N₄ and TiCl₄.S₄N₄ complexes and (b) transition metal complexes of S-atom coordinated S₄N₄H₄.

On the contrary, inorganic aromatic N-donor based ligand systems, whose electronic properties can be easily and extensively tuned by substitution of one of the elements, are still underdeveloped.^[17–19] In this connection, an underexplored class of N-donor based ligands is cyclic sulfur-nitrogen compounds. Very recently, the electronic structures of cyclic S₃N₃ have been explored by us.^[18] Interestingly, there are more than one possible coordination sites viz. lone pair electrons on N as well as on S-atoms. Besides, these compounds are usually π -electron rich. Hence, these ligands can adapt versatile bonding to stabilize the metal center in different ways, which can act a promising strategy for exploring numerous reactivity. The first transition metal complexes of cyclic SN compounds, MoCl₅.S₄N₄ and TiCl₄.S₄N₄ were synthesized and described more than 100 years ago by Davis and Wolbling (Scheme 1a).^[20,21] Later, the significant research to utilize cyclic S₂N₂ compounds as ligands to transition metal complexes have been largely developed by Dehnicke, Muller and others (Scheme 2).^[22–24] A majority of the cyclic sulfur-nitrogen complexes structurally studied to date shows that the nitrogen atoms act as donors to the transition metal fragments.^[22–24] In the majority of the S₂N₂ complexes, S₂N₂ ring acts as a η^2 -bridging ligand between two metal fragments. Nevertheless, sulfur coordinated transition metal complexes are also known, such as Ag(S₄N₄H₄)₂ and (S₄N₄H₄)M(CO)₅ (M = Cr and W) (Scheme 1b).^[25,26] However, despite being π -electron rich, sandwich complexes of sulfur-nitrogen, where cyclic π -ring is coordinated to metal, are not isolated yet. Thus, understanding the electronic structure of inorganic aromatic cyclic sulfur-nitrogen compounds as ligands and their development remains an area of great interest.



Scheme 2: Schematic representation of (a) mono- and (b-e) bi-metallic transition metal complexes of S_2N_2 .

In light of our continuing research interest on the π -electron rich inorganic aromatic compounds, we now extend our study to the ligand property of cyclic S_2N_2 with mono- and bi-metallic transition metal fragments using detailed quantum mechanical calculations. Also note that, to the best of our knowledge, all the experimentally reported S_2N_2 transition metal complexes that are known so far contains one or more halogen ligands in the S_2N_2 σ - plane (Scheme 2).^[22-24] Therefore, herein we aim to provide insight into the σ - and π -reactivity of S_2N_2 as a ligand and the role of halogens in the S_2N_2 transition metal complexes. Our results might help in expanding the ligand knowledge-base for the use of inorganic aromatic compounds in coordination chemistry.

Computational Details

All the geometries were optimized at non-local DFT level of theory using Becke's exchange functional^[27] in conjugation with Perdew's correlation functional^[28] (BP86). Basis function of triple zeta quality with two sets of polarization functions were used. This level of theory is denoted as BP86/TZ2P. Scalar relativistic effects were considered using Zeroth Order Regular Approximation (ZORA)^[29-34] and the core electrons were treated by the frozen-core approximations. The geometry optimizations were performed using ADF 2018 program package.^[35,36] The atomic charge and populations analysis were carried out by Natural population analysis implemented in Natural Bonding Orbital (NBO version 3.1),^[37] while aromatic nature of the ring system was evaluated by Nuclear Independent Chemical Shift (NICS)^[38] analysis. NBO and NICS analysis were carried out at the M06/def2-TZVPP level of theory using the Gaussian 09 program package.^[39] The electrostatic potential (ESP) of S_2N_2 molecule at molecular isosurface were created using Multiwfn version 3.6^[40] and VMD version 1.9.3^[41] softwares. Topological analysis of electron density using Bader's quantum theory of atoms in molecules (QTAIM)^[42-44] were also performed by Multiwfn 3.6^[40] program packages. Using the Gaussian 09 program package,^[39] the wavefunction file for the ESP plot and for the QTAIM analysis were generated at the M06/def2-TZVPP level of theory. QTAIM analysis is applied to describe the electronic properties of the molecules by calculating bond paths, bond critical points (BCP) and ring critical points (RCP).^[45-47] The atomic interactions are revealed by the various descriptors at the critical points such as electron density $\rho(\rho)$, laplacian of electron density $[\nabla^2]^2(r)$, potential energy density $V(r)$, kinetic energy density $G(r)$, total energy density $H(r)$ and ellipticity (ϵ). These were done by single point calculations at the meta-GGA exchange-correlation functional M06^[48] with def2-TZVPP^[49] basis set on geometries optimized at the BP86/TZ2P level of theory. The EDA-NOCV calculations were carried out using BP86/TZ2P geometries with the ADF 2018 program package.^[50,51]

The bonding nature between molecular fragments in a molecule have been investigated by means of an energy decomposition analysis (EDA, also termed extended transition state method -ETS) developed independently by Morokuma^[52] and by Ziegler and Rauk.^[53] The EDA focuses on the analysis of the instantaneous interaction energy E_{int} , which gives a quantitative picture of the chemical bond formation between fragments in

the frozen geometry of the molecule. The interaction energy (E_{int}) can be partitioned into three physically meaningful parameters, viz. electrostatic interaction (E_{elstat}), Pauli repulsion (E_{Pauli}) and orbital (covalent) interaction (E_{orb}).

$$\Delta E_{\text{int}} = \Delta E_{\text{elstat}} + \Delta E_{\text{Pauli}} + \Delta E_{\text{orb}} \quad (1)$$

E_{elstat} gives the quasiclassical electrostatic interaction between the fragments, E_{Pauli} is the repulsive exchange interaction between electrons of the fragments having same spin and E_{orb} is the orbital (covalent) interaction which comes from the orbital relaxation and the orbital mixing between the fragments. The E_{orb} term can be partitioned into contributions from orbital having different symmetries. The EDA-NOCV scheme breaks down the E_{orb} term into pairwise contributions of interacting orbitals of the two fragments. NOCV (Natural Orbital for Chemical Valence) is defined as the eigen vectors of the valence operator, \hat{V} , given by the equation:

$$\hat{V} \hat{v}_i = \epsilon_i \hat{v}_i \quad (2)$$

The total orbital interaction E_{orb} may moreover be derived from pairwise orbital interaction energies ΔE_k^{orb} that are associated with the deformation densities $\Delta \rho_k$, which is the difference between the densities of the fragments before and after bond formation.

$$E_{\text{orb}} = \sum_{k=1}^{N/2} E_k^{\text{orb}} = \sum_{k=1}^{N/2} v_k \left[-F_{-k,-k}^{\text{TS}} + F_{k,k}^{\text{TS}} \right] \quad (3)$$

The terms $-F_{-k,-k}^{\text{TS}}$ and $F_{k,k}^{\text{TS}}$ are diagonal transition-state (TS) Kohn–Sham matrix elements corresponding to NOCVs with the eigenvalues $-v_k$ and v_k , respectively. The ΔE_k^{orb} term of a specific kind of bond are allocated by visual assessment of the shape of the deformation density, $\Delta \rho_k$. The EDA-NOCV scheme in this manner, gives quantitative (ΔE_{orb}) data about the strength of orbital interactions in chemical bonds.

Results and Discussion

In order to explore the ligand property of S_2N_2 , we have studied the complex formation of S_2N_2 with one and two square pyramidal 14 valence electron $[\text{Mo}(\text{NO})\text{Cl}_4]^-$ metal fragment(s). First, we describe the electronic structure and reactivity of S_2N_2 ligand, followed by the bonding nature in mono-metallic and bi-metallic transition metal complexes. The optimized geometries of S_2N_2 , $\text{S}_2\text{N}_2[\text{Mo}(\text{NO})\text{Cl}_4]^-$ (**1Mo**) and $\text{S}_2\text{N}_2[\text{Mo}(\text{NO})\text{Cl}_4]_2^{2-}$ (**2Mo**) complexes at the BP86/TZ2P level of theory using scalar relativistic ZORA are given in figure 1. All structures are minima on the potential energy surface. The geometrical parameters of the optimized structure of S_2N_2 and **2Mo** are close to the experimentally reported geometrical parameters in the crystal structure.^[54,55] The geometrical parameters of the gas-phase structure of S_2N_2 is also close to our calculated values (Table S4).^[56]

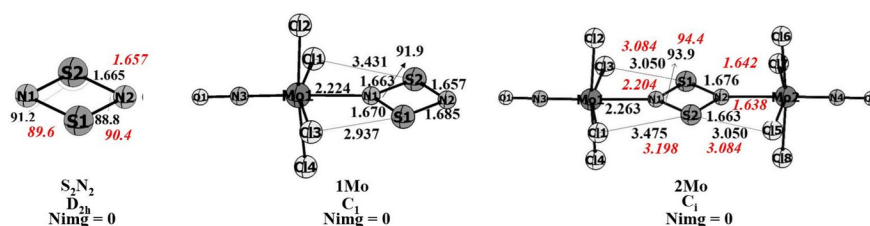


Figure 1 : Optimized geometries and important geometrical parameters of S_2N_2 , $[\text{S}_2\text{N}_2(\text{Mo}(\text{NO})\text{Cl}_4)]^-$ (**1Mo**) and $\text{S}_2\text{N}_2[\text{Mo}(\text{NO})\text{Cl}_4]_2^{2-}$ (**2Mo**) at the BP86/TZ2P/ZORA level of theory using ADF program package. Distances are given in angstroms (\AA) and angles are given in degrees ($^\circ$). The number of imaginary frequencies (Nimg) and the point group symmetry are also given. Experimental parameters from crystal structure are given in italics (red colour).

S_2N_2

The singlet $\mathbf{S}_2\mathbf{N}_2$ is more stable than the triplet state by 58.8 kcal/mol (Figure S1). Hence, we have limited our discussion on singlet $\mathbf{S}_2\mathbf{N}_2$. $\mathbf{S}_2\mathbf{N}_2$ is a near-perfect square with an equal S-N bond length of 1.665 Å and near right-angular bond angles of $\angle\text{SNS} = 88.8^\circ$ and $\angle\text{NSN} = 91.2^\circ$. Therefore, $\mathbf{S}_2\mathbf{N}_2$ shows the characteristic geometric criteria for traditionally aromatic molecules.^[57] The natural population analysis of $\mathbf{S}_2\mathbf{N}_2$ is given in table 1. The partial atomic charge on more electronegative N-atoms ($\chi_N = 3.04$)^[58] and less electronegative S-atoms ($\chi_S = 2.58$)^[58] in $\mathbf{S}_2\mathbf{N}_2$ are -0.85 e and 0.85 e. In spite of the difference in the electronegativity of N- and S-atoms, the population in the perpendicular p_z -orbital on N-atoms (1.45 e) and S-atoms (1.50 e) are comparable. This indicates a nearly uniform π -electron distribution in electron rich $6\pi\mathbf{S}_2\mathbf{N}_2$, similar to cyclic S_3N_3 systems.^[18,59] The HOMO-2 (σ_7) and HOMO (π_3) of S_2N_2 are σ - and π -molecular orbitals (MO) having major coefficient on N-atoms (Figure 2). The LUMO (σ_8) and LUMO+1 (π_4) are σ - and π -MOs having major coefficient on S-atoms. Thus, in principle, N-atom can act as σ - and π -donor while S-atom can act as σ - and π -acceptor. A S-N bond order of 1.22 in $\mathbf{S}_2\mathbf{N}_2$ indicates a reduction in the S-N double bond character and corroborates well with the description of electron rich π -systems (Table 1).^[18,59]

The Nucleus-Independent Chemical Shift (NICS) value at the ring center, NICS(0), and 1 Å above, NICS(1), and the axial components of the shielding tensor NICS(0)_{zz} and NICS(1)_{zz} indicates weakly aromatic character (Table 2). However, the low negative values of NICS(1)_{zz} indicate a relatively poor delocalization of π -electrons as compared to standard 6π aromatic systems like benzene and its analogues.^[38] Our NICS values show a parallel with the reported NICS values of $\mathbf{S}_2\mathbf{N}_2$ at a higher level of theory.^[60] Note that, Head-Gordon, Schleyer, and co-workers assigned $\mathbf{S}_2\mathbf{N}_2$ as essentially a weakly aromatic 2π electrons system based on structural, energetic and magnetic criteria.^[61]

Table 1 : Atomic partial charge distribution, atomic orbital population and bond order given by the natural population analysis for $\mathbf{S}_2\mathbf{N}_2$, $\text{S}_2\text{N}_2[\text{Mo}(\text{NO})\text{Cl}_4]^-$ (**1Mo**) and $\text{S}_2\text{N}_2[\text{Mo}(\text{NO})\text{Cl}_4]_2^{2-}$ (**2Mo**) at the M06/def2-TZVPP level of theory by Gaussian G09 program package.

	Natural Charge ^a	Natural Charge ^a	Population in p_z ^b	Population in p_z ^b	Bond Order ^c
$\mathbf{S}_2\mathbf{N}_2$	$q(\text{S})$ 0.85	$q(\text{N})$ -0.85	(S) 1.50	(N) 1.45	P(S-N) 1.22
1Mo	S1 = 0.96 S2 = 0.94	N1 = -0.93 N2 = -0.87	S1 = 1.47 S2 = 1.46	N1 = 1.57 N2 = 1.42	N1-S1 = N1-S2 = 1.10 N2-S2 = 1.25 N2-S1 = 1.19
2Mo	S1 = S2 = 1.05	N1 = N2 = -0.93	S1 = S2 = 1.43	N1 = N2 = 1.54	N1-S1 = N2-S2 = 1.10 N1-S2 = N2-S1 = 1.13

^a q represents charge on the individual atoms. ^b population on each p_z atomic orbital in the compound. ^c bond order calculated by natural population analysis.

Table 2: Nucleus-Independent Chemical Shift (NICS) analysis of $\mathbf{S}_2\mathbf{N}_2$ and S_2N_2 ring in $\text{S}_2\text{N}_2[\text{Mo}(\text{NO})\text{Cl}_4]^-$ (**1Mo**) and $\text{S}_2\text{N}_2[\text{Mo}(\text{NO})\text{Cl}_4]_2^{2-}$ (**2Mo**) at the M06/def2-TZVPP level of theory.

	NICS(0) ^a	NICS(0) _{zz} ^b	NICS(1) ^a	NICS(1) _{zz} ^b
$\mathbf{S}_2\mathbf{N}_2$	2.85	66.99	-1.62	-1.49
1Mo	8.28	47.04	-24.38	2.24
2Mo	-8.47	-40.03	-6.64	-6.95

^a NICS(0) and NICS(1) represent NICS values at the center of and 1 Å above the four-membered rings.^b NICS(0)_{zz} and NICS(1)_{zz} represent the out-of-plane component of shielding tensor at the center of and 1 Å above the four-membered rings.

We have further analyzed the strength of the π bonding of $\mathbf{S}_2\mathbf{N}_2$ ring using the EDA–NOCV analysis. Frenking and co-workers have used the energy decomposition analysis (EDA) as a powerful tool for investigating the conjugation and aromaticity in carbocyclic and heterocyclic systems.^[62,63] The EDA–NOCV analysis of $\mathbf{S}_2\mathbf{N}_2$ is carried out using the fragmentation pattern shown the scheme S1, where the S–N bond was fragmented homolytically in two quartet SN fragments in the frozen geometry of the molecule $\mathbf{S}_2\mathbf{N}_2$ for this purpose (Scheme S1). Since S–N single-bond has σ symmetry, the π contributions to the total orbital interactions (ΔE_π) can be considered as a measure for the π -electron delocalization as compared to the respective fragments.^[18] The negative interaction energies ΔE_{int} indicates stabilizing interaction between the fragments for the formation of $\mathbf{S}_2\mathbf{N}_2$ (Table 3). The major contribution to the total interaction, ΔE_{int} , comes from the orbital term ΔE_{orb} (62.8%), indicating a strong covalent bonding. The breakdown of ΔE_{orb} into pairwise orbital interactions shows that the bonding interaction between the fragments comes mainly from the σ -interaction (ΔE_σ , 87.5%) between the respective quartet fragments. However, the contribution for the π -interaction is significant (-73.2 kcal/mol) and contributes 10.6% to the total ΔE_{orb} . The EDA results indicate the nature of π -interaction in π electron-rich cyclic sulfur-nitrogen systems $\mathbf{S}_2\mathbf{N}_2$ and $\mathbf{S}_3\mathbf{N}_3$ are similar.^[18]

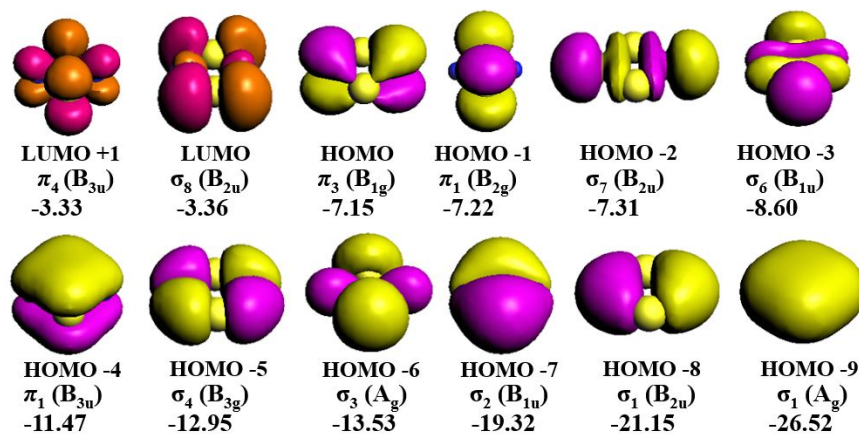


Figure 2: Important molecular orbitals of the $\mathbf{S}_2\mathbf{N}_2$ at the BP86/TZ2P/ZORA level of theory, generated using ADF program package. Energies eigen values are given in eV.

Table 3: EDA results for the estimation of the π -interaction in $\mathbf{S}_2\mathbf{N}_2$ and $\mathbf{S}_2\mathbf{N}_2$ ring in **1Mo** and **2Mo** at the BP86/TZ2P/ZORA level of theory according to the fragmentation pattern described in Scheme S1. Energies are in kcal/mol.

	ΔE_{int}	ΔE_{orb}	ΔE_{elstat} ^a	ΔE_{exch} ^a	$\Delta E_{\text{orb}}^\beta$	$\Delta E_{\text{int}}^\beta$	$\Delta E_{\text{elstat}}^\beta$
$\mathbf{S}_2\mathbf{N}_2$	-219.2	871.1	-397.8 (36.5%)	-692.5 (63.5%)	-606.1 (87.5%)	-73.2 (10.6%)	-13.2 (1.9%)
1Mo	-255.1	864.8	-404.6 (36.1%)	-715.3 (63.9%)	-613.5 (85.8%)	-79.5 (11.1%)	-22.3 (3.1%)
2Mo	-244.9	903.7	-375.3 (32.7%)	-773.3 (67.3%)	-667.8 (86.4%)	-81.0 (10.5%)	-24.5 (3.1%)

^a The percentage values in parentheses give the contribution to the total attractive interactions $\Delta E_{\text{elstat}} +$

ΔE_{orb} .^b The percentage values in parentheses give the contribution to the total orbital interactions ΔE_{orb} .

S_2N_2 shows four bond critical points (BCPs) for each of the four S-N bonds and a ring critical point (RCP) at the center (Figure 3a). The BCPs are relatively close to S-atoms, indicating bond polarization. The electron density $\rho(r)$ and the Laplacian of the electron density $\nabla^2(r)$ at the BCPs indicate the accumulation of electrons and thus a covalent nature of the bonds (Table 4). The negative total energy density $H(r)$ at the BCP also supports covalent nature.^[64] A high ϵ value for S-N bonds also indicates multiple bond character due to the presence of π -delocalization. Likewise, a substantial value of $\rho(\rho)$ and $\nabla^2(r)$ at the RCP indicates possible delocalization of electrons,^[65] which can be correlated with the negative NICS(1)_{zz} values (Table 2). Contour line diagram of the Laplacian distribution of the electron density $\nabla^2(r)$ of the S_2N_2 is also shown in figure 3a. Solid lines represent the areas of electronic charge concentration, while dashed lines show areas of charge depletion. The shape of the Laplacian distribution clearly shows that N atoms of the S_2N_2 ring have an area of charge concentration and S atoms of the S_2N_2 ring have an area of charge depletion along the extension of the S-N covalent bonds.

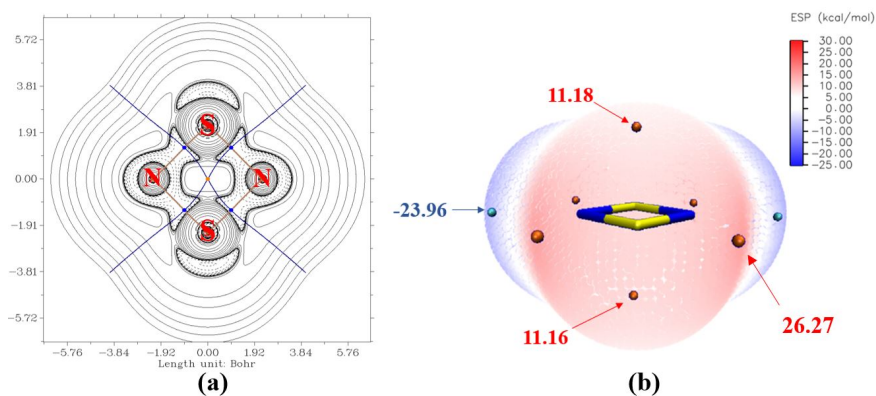


Figure 3: (a) Contour maps of the Laplacian distribution of electron density in the plane of S_2N_2 molecule. Dashed lines indicate regions of electronic charge concentration ($\nabla^2(r) < 0$), and solid lines denote regions of electronic charge depletion ($\nabla^2(r) > 0$). Small blue spheres represent bond critical points (BCPs) and small orange sphere represent ring critical point (RCP). Bond paths and interatomic surface paths are indicated by brown and blue lines. (b) Molecular electrostatic potential mapped on the molecular surface of S_2N_2 . Blue indicates N-atom and yellow indicates S-atom. Red color represents accumulation of positive charge and blue color indicates accumulation of negative charge. Surface local minima (V_{min}) and maxima (V_{max}) of ESP in kcal/mol are represented as cyan and orange spheres, respectively.

In order to further understand the reactivity of S_2N_2 molecule we have calculated the electrostatic potential (ESP) map on the molecular van der Waals surface (Figure 3b). The ESP plot shows that both electrophilic and nucleophilic regions are present on S_2N_2 molecular surface. The region of negative ESP is present in the direction of the lone pair of the nitrogen atoms. The region of positive ESP is observed in the plane of S_2N_2 around S-atom along the extension of the covalent S-N bonds. In addition, a positive region at the center of the ring in the direction perpendicular to the σ -plane of S_2N_2 is observed. This shows excellent correspondence with the QTAIM analysis in figure 3a. Thus, one can expect S_2N_2 might act as σ -donor through N-atom and S-atom have both σ - and π -hole,^[66] which rationalizes the versatility of S_2N_2 as a ligand. Thus, S_2N_2 could be exploited in transition metal chemistry as a ligand. Also, the existence of halogen-S interaction in the transition metal complex of S_2N_2 is known.^[23] Interactions between π -hole of S_2N_2 and the Lewis bases such as NH_3 , PH_3 and AsH_3 is theoretically reported.^[67] However note that any attempt to optimize sandwich complexes of S_2N_2 , where the cyclic π -ring is coordinated with different transition metal fragments were not successful (Table S1). This corroborates well the non-existence of such complexes experimentally.

Table 4: Topological parameters of the electron density at the bond critical points (BCPs) and ring critical points (RCPs) of $[\text{S}_2\text{N}_2(\text{Mo}(\text{NO})\text{Cl}_4)]^-$ (**1Mo**) and $[\text{S}_2\text{N}_2(\text{Mo}(\text{NO})\text{Cl}_4)_2]^{2-}$ (**2Mo**) calculated at the M06/def2-TZVPP level of theory. Electron density $\rho(\rho)$, Laplacian of electron density $\nabla^2(r)$, Potential energy density $V(r)$, Kinetic energy density $G(r)$ and Total energy density $H(r)$ in a. u.

	BCP/RCP	$\rho(\rho)$	$\nabla^2(r)$	$V(r)$	$G(r)$	$H(r)$	$G(r)/V(r)$	ϵ
S₂N₂	S-N	0.2241	-0.3568	-0.4133	0.1621	-0.2513	0.3922	0.4712
	S ₂ N ₂ ^a	0.0906	0.3044	-0.1190	0.0976	-0.0215	0.8202	-1.4832
1Mo	Mo-N1	0.1058	0.1683	-0.1315	0.0868	-0.0447	0.6601	0.0275
	S1-N1	0.2202	-0.3377	-0.4086	0.1621	-0.2465	0.3967	0.5130
	S1-N2	0.2156	-0.3453	-0.3767	0.1452	-0.2315	0.3855	0.4582
	N1-S2	0.2222	-0.3258	-0.4204	0.1695	-0.2509	0.4032	0.4873
	N2-S2	0.2263	-0.3284	-0.4334	0.1757	-0.2578	0.4054	0.4623
	S1-Cl3	0.0222	0.0603	-0.0138	0.0144	0.0007	1.0435	0.0624
	S ₂ N ₂ ^a	0.0863	0.3182	-0.1158	0.0977	-0.0182	0.8437	-1.5122
	MoNSCl ^a	0.0185	0.0726	-0.0143	0.0162	0.0019	1.1329	-2.8828
2Mo	Mo1-N1/ Mo2-N2	0.0985	0.1314	-0.1177	0.0753	-0.0424	0.6398	0.0318
	S1-N1/ S2-N2	0.2217	-0.3121	-0.4236	0.1727	-0.2508	0.4077	0.5003
	N1-S2/ N2-S1	0.2163	-0.3180	-0.3978	0.1591	-0.2386	0.3999	0.4829
	S1-Cl3/ S2-Cl5	0.0175	0.0517	-0.0106	0.0118	0.0012	1.1132	0.1597
	S ₂ N ₂ ^a	0.0848	0.3264	-0.1149	0.0983	-0.1667	0.8555	-1.5612
	MoNSCl ^a	0.0156	0.0603	-0.0115	0.0133	0.0017	1.1565	-2.5578

^a represents four-membered rings, having a ring critical point.

S₂N₂[Mo(NO)Cl₄]⁻

(1Mo)

The bonding interaction of S₂N₂ with the metal fragment can be better understood from the fragment orbital analysis of [Mo(NO)Cl₄]⁻. The fragment [Mo(NO)Cl₄]⁻ is square pyramidal in structure and a valence electron count ascertains that it has 14 valence electrons. The metal centric fragment orbitals available for bonding in the 14 VE transition metal square pyramidal ML₅ fragment are shown in scheme 3. The eight d metal electrons can occupy *b*₂, *e* and *b*₁ set of orbitals, leaving the *a*₁ orbitals that can accept lone pair from N in S₂N₂ to form Mo-N σ -bond. Thus, HOMO-2 of S₂N₂ majorly concentrated on N has the right symmetry to donate to *a*₁ fragment d-orbital and the perpendicular π -type *e* fragment d-orbital is likely to donate back to the LUMO+1 (S-N π^* -MO) of the S₂N₂ to form **1Mo** (Figure 2). Thus, the bonding in **1Mo** can be qualitatively regarded as similar to Dewar-Chatt-Duncanson model of σ -donation from ligand to metal and π -back donation from metal to ligand.^[68,69] However, a detailed bonding analysis will be helpful in examining the relative strength and effect of these interactions in a more quantitative way.

Scheme 3: Schematic representation of the d-orbitals in a square pyramidal ML₅ fragment.

The optimized geometry of **S₂N₂[Mo(NO)Cl₄]⁻ (1Mo)** is shown in figure 1. The four membered S₂N₂ ring is planar in **1Mo**, having unequal S-N bond lengths. The S1-N1 and S1-N2 bonds are longer, while S2-N1 and S2-N2 bond length is comparable to S-N bond length in S₂N₂ molecule. The S1-N1 (1.670 Å) and S1-N2 (1.685 Å) bond elongation can be correlated with the back-donation of electrons from the metal fragment

to S_2N_2 π^* -MO. The bond angle at N-atoms increases from 88.7° in S_2N_2 to 91.9° in $\mathbf{1Mo}$ to facilitate metal coordination. Furthermore, the S1...Cl3 distance (2.937 Å) is within the sum of the van der Waals radius of Cl and S-atoms (3.55 Å),^[70] indicating a non-covalent type intramolecular interaction between Cl3 and S1. This rather short S-Cl distance is already noted by Dehnicke and coworkers in many bi-metallic complexes of N_2S_2 .^[23] Hence, the σ -hole at the chalcogen atom receives the electron pair from Cl and thus plays a crucial role in the chalcogen bond formation between Cl and S.^[71,72] The molecular orbital analysis identifies HOMO-12, HOMO and HOMO-1 as N-Mo σ -donation, Mo-N π -back donation, and S1...Cl3 interaction, respectively (Figure 4).

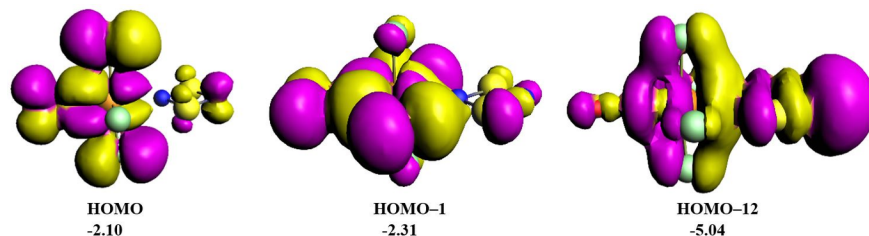


Figure 4: Important molecular orbitals of the $\text{S}_2\text{N}_2[\text{Mo}(\text{NO})\text{Cl}_4]^-$ ($\mathbf{1Mo}$). Energy eigen values are in eV. The isosurface values for molecular orbitals are 0.01 e/bohr³.

Group charge analysis in $\mathbf{1Mo}$ (Table 1) by the natural population indicates a slight positive group charge of S_2N_2 (0.10 e), suggesting net electron transfer from S_2N_2 ligand to the metal fragment. The Wiberg bond indices reveal significant reduction for S1-N1 and S1-N2 bond order (1.10) as compared to that of S-N bond order in S_2N_2 molecule (1.22), while the S2-N1 and S2-N2 bond order remains almost the same as that in S_2N_2 . This supports the variable S-N bond distances in $\mathbf{1Mo}$ (Figure 1). The atomic orbital population in the p_z -orbital of N1 is slightly higher (1.57) as compared to the population in the p_z -orbitals of N2, S1 and S2. This increase in the population could be correlated to the back donation from metal fragment to S-N π^* -MO. Thus, the bond order and population analysis suggest metal fragment to S-N π^* -back donation, which in turn gives rise to polarization in the S_2N_2 π -electron density. In addition, the second-order perturbation analysis by NBO on $\mathbf{1Mo}$ complex shows donation of chloride (Cl3) lone pair to S1-N2 σ^* -MO (5.2 kcal/mol), which is well complemented with the shorter Cl3...S1 distance. Here, the S-atom acts as acceptor in the Cl-S chalcogen bond.^[71,72] The uneven distribution of π -electrons in the p_z -orbitals of N- and S-atoms is further supported by positive NICS(1)_{zz} value (Table 2), which indicates non-aromatic character of S_2N_2 ligand in $\mathbf{1Mo}$. The ESP plot on the molecular van der Waals surface of $\mathbf{1Mo}$ shows negative potential at the metal fragment and relatively slight positive potential on S_2N_2 , supporting the positive group charge of S_2N_2 (Figure 5b).

In order to understand the π -bonding strength of S_2N_2 ring in the $\mathbf{1Mo}$ EDA-NOCV analysis were carried out using quartet SN and $\text{SN}[\text{Mo}(\text{NO})(\text{Cl})_4]^-$ fragments (Scheme S1). The bonding interaction between the $\text{SN}[\text{Mo}(\text{NO})(\text{Cl})_4]^-$ and SN fragments has 36.1% electrostatic and 63.9% covalent character. The E_{orb} has contributions from 85.8% σ -type interactions and 11.1% π -type interactions. The value of ΔE_π suggests that π bonding strength of S_2N_2 ring in $\mathbf{1Mo}$ is higher than the S_2N_2 molecule. The inspection of the deformation density plot ($\Delta\rho_2$ in Figure S7) indicates that the increase in ΔE_π in $\mathbf{1Mo}$ as compared to S_2N_2 might arise due to the donation of π -electron density from metal fragment to the S-N π^* -MO, which has more coefficient on N1. Thus the donation of electron from the metal fragment to the S-N π^* -MO would not lead to uniform π -electron distribution in the S_2N_2 ring and can not be taken as an increase in the aromaticity of $\mathbf{1Mo}$. This is also supported by higher population of the p_z -orbital on N1 (Table 1) and lower aromaticity (Table 2) of $\mathbf{1Mo}$.

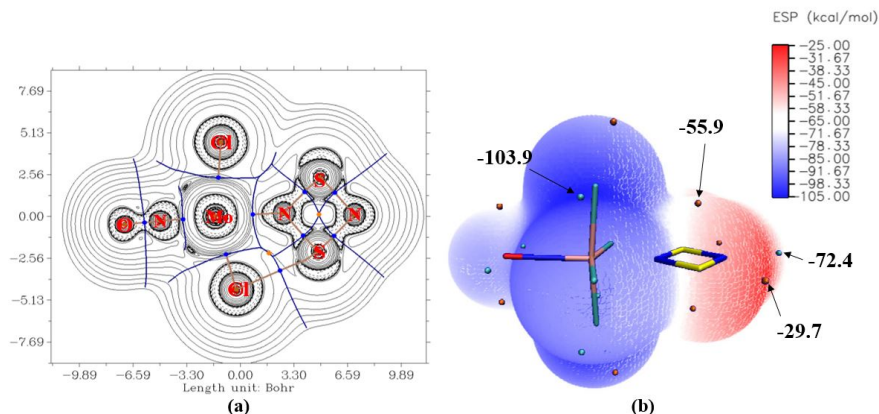


Figure 5 : (a) Contour maps of the Laplacian distribution of electron density in the plane of S_2N_2 in **1Mo** molecule. Dashed lines indicate regions of electronic charge concentration ($\nabla^2(r) < 0$), and solid lines denote regions of electronic charge depletion ($\nabla^2(r) > 0$). Small blue spheres represent bond critical points (BCPs) and small orange sphere represent ring critical point (RCP). Bond paths and interatomic surface paths are indicated by brown and blue lines. (b) Molecular electrostatic potential mapped on the molecular surface of **1Mo**. Blue indicates N-atom and yellow indicates S-atom. Red color represents accumulation of positive charge and blue color indicates accumulation of negative charge. Surface local minima (V_{\min}) and maxima (V_{\max}) of ESP in kcal/mol are represented as cyan and orange spheres, respectively.

Four BCPs and one RCP are observed in the coordinated S_2N_2 ring in **1Mo**. The $\rho(\rho)$ and $\nabla^2(\rho)$ at the BCP between S and N atoms and at the RCP in S_2N_2 ring remains close to that observed in S_2N_2 (Table 3). The electron density at the BCP ($\rho(\rho)$) between Mo and N1 is significantly higher (0.1058 a. u.) and the Laplacian of electron density ($\nabla^2(\rho)$) is positive (0.1683 a. u.), which indicates a strong electrostatic interaction between Mo and N1. However, negative $H(r)$ and $-G(r)/V(r)$ values indicate important contribution from covalent interaction as well. The inspection of the contour plot indicates depletion of charge density from N-atom as well as from Mo along the Mo-N1 bond, thus indicating donation and back donation interaction. QTAIM analysis also shows the existence of a BCP between Cl3 and S1 in **1Mo** complex ($\rho(\rho)$ and $\nabla^2(\rho)$ are 0.0222 a. u. and 0.0603 a. u. respectively), where the bond path passes through the possible σ -hole near the S-atom along the extension of S-N bond. In addition, an RCP at the center of Mo-N1-S1-Cl3 is also observed. Small positive $H(r)$ and higher $-G(r)/V(r)$ at the Cl3...S1 BCP identifies Cl-S interaction as majorly non-covalent. The role of σ -hole in stabilizing such interaction are also reported.

Scheme 4: Schematic representation of the different possible bonding interactions between metal fragment group orbitals and S_2N_2 ligand group orbitals in **1Mo** chosen for EDA-NOCV analysis. Up and down arrows indicate electrons with opposite spin and the single headed arrow (\rightarrow) indicates donor acceptor interactions between fragments.

EDA-NOCV analysis using ADF 2018 program package has been carried out to understand the quantitative nature of bonding between the transition metal fragment and S_2N_2 (Table 5). The bonding possibility in scheme 4 represents the interaction between neutral S_2N_2 ligand and 14 electron metal fragment, $[Mo(NO)Cl_4]^-$ in **1Mo** complex. The bonding possibility in scheme 4 represents two donor-acceptor interactions viz. from N lone pair to transition metal fragment (σ_1) and from metal fragment to the π^* -MO of S_2N_2 (π_1).

Table 5: EDA results of the possible bonding representation for the Mo-N bond in $S_2N_2[Mo(NO)Cl_4]^-$ (**1Mo**) and $S_2N_2[Mo(NO)Cl_4]_2^{2-}$ (**2Mo**) at the BP86/TZ2P/ZORA level of theory according to the fragmentation described in scheme 3 and 4. Energies are in kcal/mol.

	$\Delta E_{\nu\tau}$	$\Delta E_{\Pi\alpha\upsilon\lambda\iota}$	$\Delta E_{\varepsilon\lambda\sigma\tau\alpha\tau}^a$	$\Delta E_{\sigma\rho\beta}^a$	ΔE_{σ}^β	ΔE_{π}^β	$\Delta E_{\rho\varepsilon\sigma\tau}$	$\Delta E_{\pi\rho\varepsilon\pi}$	-D
1Mo	-23.0	95.8	-76.1 (64.1%)	-42.7 (35.9%)	-33.9 (79.4%)	-5.0 (11.7%)	-3.8 (8.9%)	29.0	6.1
2Mo	-46.6	160.9	-135.0 (65.1%)	-72.5 (34.9%)	-56.8 (78.3%)	-7.6 (10.5%)	-8.1 (11.2%)	98.8	52

^a The percentage values in parentheses give the contribution to the total attractive interactions $\Delta E_{\text{elstat}} + \Delta E_{\text{orb}}$. ^b The percentage values in parentheses give the contribution to the total orbital interactions ΔE_{orb} .

The bonding interaction between the metal fragment and S_2N_2 ligand has 64.1% electrostatic and 35.9% covalent character, which is in good agreement with the QTAIM and NBO analysis (Tables 1 and 3). The E_{orb} has contributions from three major donor-acceptor interactions, that is, two σ -type interactions and one π -type interaction (Figure 6). The two σ interactions contribute 69.3% of the total orbital interaction energy. The deformation density plot, ρ_1 and ρ_2 mainly correspond to the donation from σ -MO of S_2N_2 mainly localized on N-atom (lone pair) to the a_1 fragment orbital of the metal fragment (Figure 6). A careful visual inspection of ρ_1 as well as ρ_2 suggests accumulation of electron density on S1 and depletion of electron density from Cl3, which represents a donation from lone pair of electrons from Cl3 (HOMO-1 of $[\text{Mo}(\text{NO})\text{Cl}_4]^-$, Figure S2) to the S_2N_2 σ^* -MO (LUMO in Figure 2). This can be corroborated with σ -hole interaction between an electrophilic region of a S atom with a Lewis base like Cl-atom in the same molecular entity.^[71] Thus, the longer S1-N2 bond length and the less positive charge on S1 can be recognized from this interaction. On the other hand, the deformation density plot ρ_3 corresponds to the π -back-donation from the transition metal fragment to the S_2N_2 π^* -molecular orbital. This interaction contributes only 8.2% of the total orbital interaction energy. Hence, S_2N_2 in **1Mo** can act as a strong σ -donor and weak π -acceptor ligand, which is similar to N-heterocyclic aromatics like pyridines.^[6,9] Furthermore, it can also act as σ -acceptor at the S-atom by the charge transfer of N lone pair to S_2N_2 σ^* -MO. In order to investigate the π -donation property of S_2N_2 , we have carried out the EDA-NOCV analysis on the theoretically modeled electron-deficient 12 valence electron fragment $[\text{Mo}(\text{NO})\text{Cl}_4]^+$ with the S_2N_2 ligand (Table S2, Figure S4).^[73] The EDA analysis indicates a substantial contribution (25%) of the π -donation from S_2N_2 π -MO (HOMO in Figure 2) to the e-type metal fragment orbital. The σ -donation from S_2N_2 σ -MO (HOMO-1 in Figure 2) to the a_1 -type metal fragment orbital contributes 45.9% to the orbital interaction. Thus, in the presence of suitable metal fragment S_2N_2 can also act as π -donor ligand (Table S2).^[73]

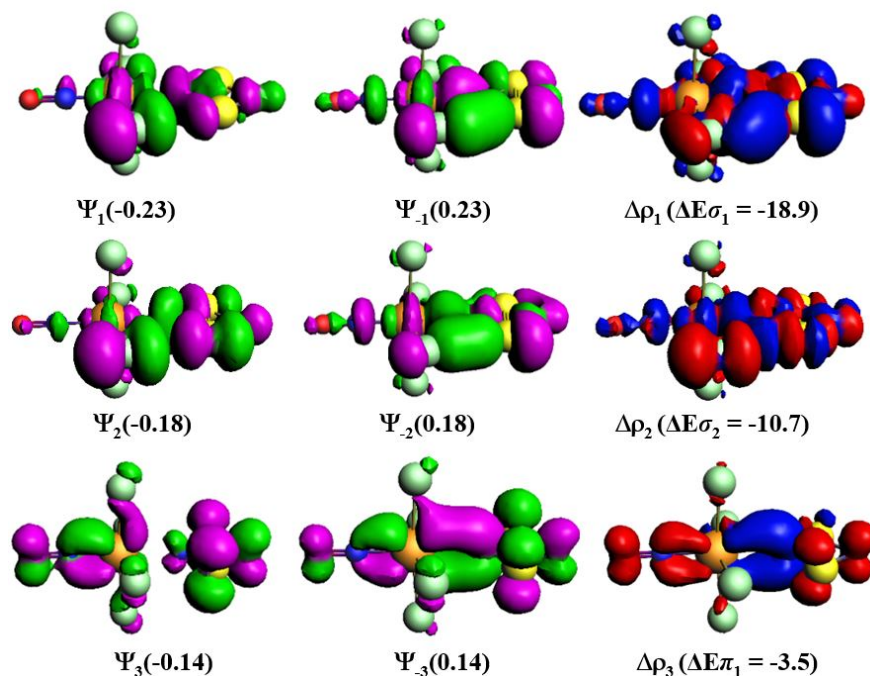


Figure 6 . Plots of NOCV pair of orbitals Ψ_{-n}/Ψ_n of π and σ bonding possibility in $\text{S}_2\text{N}_2[\text{Mo}(\text{NO})\text{Cl}_4]^{2-}$ with their eigen values in the parenthesis, the associated deformation densities $\Delta\rho_n$ and the orbital stabilization energies ΔE (in kcal/mol) at the BP86/TZ2P/ZORA level of theory. The direction of the charge flow in the deformation density plot $\Delta\rho_n$ is from red-blue. The isosurface values for NOCV orbitals and deformation densities are 0.03 and 0.0003 respectively.

$\text{S}_2\text{N}_2[\text{Mo}_2\text{Cl}_8(\text{NO})_2]^{2-}$ (2Mo)

In $\text{S}_2\text{N}_2[\text{Mo}(\text{NO})\text{Cl}_4]_2^{2-}$ (2Mo), S_2N_2 molecule act as a η^2 -bridging ligand between two $\text{Mo}(\text{NO})\text{Cl}_4^-$ fragments. The crystal structure of this compound is reported by Dehnicke and co-workers in the year 1987.^[74] It is expected that the bonding and *anti*-bonding combination of two a_1 -orbitals (Scheme 3) from two metal fragments can accept the lone pairs from two N-atoms and bonding combination of the two π -type perpendicular e -orbitals would be engaged in a multi-centre π -back donation to the S-N π^* -MO (LUMO +1, π_4 in Figure 2). Figure 1 shows the optimized geometry of $\text{S}_2\text{N}_2[\text{Mo}(\text{NO})\text{Cl}_4]_2^{2-}$. The geometrical parameters of the optimized structure of 2Mo are close to the experimentally reported geometrical parameters (Table S4).^[74] Here, S_2N_2 ring is planar with a rectangular shape, where N1-S2 and N2-S1 bonds are slightly longer (1.676 Å) than N1-S1 and N2-S2 bonds (1.663 Å), which is close to S-N bond length in S_2N_2 . Analogous to 1Mo, an increase in bond angles at N-atom is observed in 2Mo (93.9deg) to facilitate metal coordination at N-atoms. The S1***Cl3 and S2***Cl5 distance are relatively shorter (3.050 Å) than S1***Cl7 and S2***Cl11 distance (3.475 Å) indicating possible non-covalent interactions between chloride and sulphur atoms in the complex, as noted by Dehnicke and coworkers.^[23] This interaction can be correlated to the σ -hole present at S-atom. The HOMO-26 shows N-Mo σ -donation and HOMO-1 shows Mo-N back donation (Figure 7). In addition, the S...Cl interaction can be observed in HOMO-3.

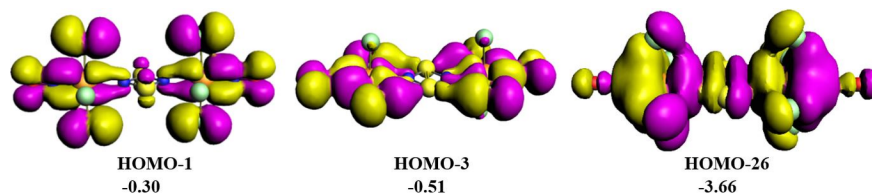


Figure 7 : Important molecular orbitals of the $\text{S}_2\text{N}_2[\text{Mo}(\text{NO})\text{Cl}_4]_2^{2-}$ (**2Mo**) . Energy eigenvalues are in eV. The isosurface values for molecular orbitals are 0.01 e/bohr³.

NBO charge and population analysis (Table 1) were performed to gain a more detailed insight into the electronic structure of **2Mo** as well as on the nature of S_2N_2 as a bridging ligand. The positive group charge on S_2N_2 ring (0.24 e) indicates a higher extent of the net donation from S_2N_2 bridging ligand to the two metal fragments as compared to **1Mo** . The Wiberg bond indices of all the S-N bonds reduced significantly as compared to S_2N_2 , which manifests donation from filled d-orbitals of metal fragments to the anti-bonding π^* -molecular orbitals of S_2N_2 ligand. It is interesting to note that, the overall atomic population in the perpendicular p_z -orbitals on S and N is similar to that observed in S_2N_2 . However the atomic population in the perpendicular p_z -orbitals on N atoms (1.54 e) has increased and that in the perpendicular p_z -orbitals on the S-atoms has decreased (1.43 e). This clearly denotes a significant π -back donation from the metal fragments to the π^* -MO of S_2N_2 ring (LUMO, π_4 in Figure 2). Thus, even though the total population in the π -orbitals of S_2N_2 in **2Mo** remains similar to free S_2N_2 , we can observe a reversal of the direction of polarization of the π -electron density in **2Mo** . The second order perturbation theory analysis by NBO on **2Mo** shows a significant donation from lone pair of chloride ligands (Cl3/Cl7) to S1-N2/S2-N1 σ^* -orbitals (3.7 kcal/mol), which is well complemented with the Cl3...S1/Cl5...S2 distances in the geometrical analysis. This interaction is similar to the chalcogen bonding described by Cremer and co-workers.^[71]

The higher negative NICS(1)_{zz} value observed for the S_2N_2 ring in **2Mo** corroborates with the increase in the π -electron density due to back donation from the metal fragment (Table 2). The more negative ESP on the metal fragments as compared to the S_2N_2 ring, however, indicates a net transfer of electrons to the metal fragments validating the positive charge on S_2N_2 (Figure 8b). In order to understand the π bonding strength of S_2N_2 in **2Mo** , the elongated S-N bonds (S1-N2 and S2-N1) are cleaved leading to two quartet $\text{SN}[\text{Mo}(\text{NO})(\text{Cl})_4]^-$ fragments (Scheme S1). The major contributions to the total orbital interaction energy (ΔE_{orb}), between the fragments is higher than for the S_2N_2 molecule implying greater covalent character (Table 3). Also, the π -contribution to the orbital interactions are -81.0 kcal/mol in **2Mo** and -73.2 kcal/mol in S_2N_2 molecule. Thus, the π bonding strength of S_2N_2 in the **2Mo** is more than the π bonding strength of S_2N_2 molecule. The inspection of the deformation density plot ($\Delta\rho_2$ in Figure S8) exhibits depletion of electron density from the two metal fragments to the S_2N_2 ring. Thus, the double donation makes an uniform increase of the π -electron density in the S_2N_2 ring in **2Mo** as compared to S_2N_2 ring in **1Mo** . Therefore, an uniform increase in the population of p_z -orbitals (Table 1) and higher aromatic character (Table 2) of **2Mo** is validated.

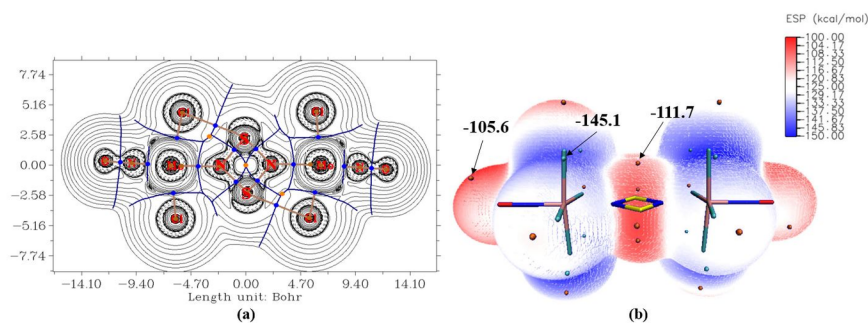


Figure 8: (a) Contour maps of the Laplacian distribution of electron density in the plane of **2Mo** molecule. Dashed lines indicate regions of electronic charge concentration ($\nabla^2(r) < 0$), and solid lines denote regions of electronic charge depletion ($\nabla^2(r) > 0$). Small blue spheres represent bond critical points (BCPs) and small orange sphere represent ring critical point (RCP). Bond paths and interatomic surface paths are indicated by brown and blue lines. (b) Molecular electrostatic potential mapped on the molecular surface of **2Mo**. Blue indicates N-atom and yellow indicates S-atom. Red color represents accumulation of positive charge and blue color indicates accumulation of negative charge. Surface local minima (V_{\min}) and maxima (V_{\max}) of ESP in kcal/mol are represented as cyan and orange spheres, respectively.

QTAIM analysis of **2Mo** reveals the existence of four BCPs in between four S-N bonds and a ring critical point at the center of the S_2N_2 ring (Figure 8a). The $\rho(\rho)$ and $\nabla^2(r)$ values for the BCPs and RCP of S_2N_2 ring in **2Mo** are very similar to that in S_2N_2 ring in **1Mo** (Table 3). Two BCPs are observed between Mo1-N1 and Mo2-N2 bonds, which have similar electronic characteristics as observed for the Mo-N1 bond in **1Mo** (Table 3). Similar to **1Mo**, charge depletion from N-atom to Mo as well as from Mo to N is also observed in the contour plot of Laplacian distribution of the electron density of **2Mo** indicating N-Mo donation and Mo-N back donation. Moreover, two BCPs are observed between S1...Cl3 and S2...Cl5, where the bond path passes through the σ -hole of S-atom. This interaction is similar to the chalcogen bonding between sulfur and chlorine atom in various other systems facilitated by σ -hole on S-atom.^[71] In addition, two RCPs were also observed at the center of two Mo-N-S-Cl rings. Note that, the AIM descriptors at these BCPs are similar to the BCPs of **1Mo**. This indicates similarity in the chemical bonding of S_2N_2 with one and two transition metal fragments.

Scheme 5: Schematic representation of the possible bonding interaction between metal fragment group orbitals and S_2N_2 ligand group orbitals in **2Mo** chosen for EDA-NOCV analysis. Up and down arrows indicate electrons with opposite spin and the single headed arrow (\rightarrow) indicates donor acceptor interactions between fragments.

In order to understand the quantitative bonding interaction between two $[Mo(NO)Cl_4]^-$ fragments and bridging S_2N_2 in the frozen geometry of **2Mo**, EDA-NOCV analysis implemented in ADF 2018 program package were carried out (Table 5). The fragmentation scheme is given in scheme 5, which indicates two donor-acceptor N-Mo σ -interactions and one donor-acceptor Mo-N π -back donation. Table 5 shows the calculated EDA results for the interaction between $[Mo_2(NO)_2Cl_8]^{2-}$ fragment and neutral $\eta^2-S_2N_2$ bridging ligand. The major contribution to the total interaction energy, E_{int} comes from the electrostatic interaction, E_{elstat} (65.1%) rather than covalent interaction ΔE_{orb} (34.9%). The breakdown of ΔE_{orb} into pairwise orbital interactions shows that the bonding interaction between the fragments comes mainly from the σ -interaction (ΔE_{σ} , 72.5%) between the respective singlet fragments. The deformation density plots correspond to three σ -interactions viz. ρ_1 , ρ_2 and ρ_3 (Figure 9). The ρ_1 and ρ_3 correspond to the donation from *anti*-bonding and bonding combination of lone pair orbitals on N atoms in S_2N_2 ligand to the *anti*-bonding and bonding combination of the fragment orbitals of $[Mo_2(NO)_2Cl_8]^{2-}$. The ρ_2 corresponds to donation from in-plane Cl ligand attached to the metal center to the S_2N_2 σ^* -MO. This can be correlated with the Cl to S σ -hole interaction.^[71] The deformation density plot ρ_4 corresponds to the π -back-donation from the transition metal fragment to the S_2N_2 π^* -molecular orbital. This interaction contributes 7.8% of the total orbital interaction energy. Thus, S_2N_2 acts mainly as a strong σ -donor and weak π -acceptor both as a mono- and bi-dentate ligand. Note that, the percentage contribution of the σ - and π -interaction to the total E_{orb} is similar in mono- and bi-metallic complexes (Table 5). However, the absolute value of these interactions in **2Mo** is roughly double than that in **1Mo**. The major difference in the η^2 -coordination vs η^1 -coordination is observed in the higher dissociation energy of **2Mo** (52.3 kcal/mol) as compared to **1Mo** (6.1 kcal/mol), corroborating with the experimental isolation of a higher number of bi-metallic complexes (Scheme 2).^[22-24] This nature of ligand is quite similar to heterocycles such as pyrazine in organometallic chemistry.^[75] However interestingly, S_2N_2 can also acts as a σ -acceptor due to the presence of electro-positive S-atom, which can lead to additional stability to the transition metal complexes of S_2N_2 with appropriate donor ligands at the metal center. We have also studied the π -donation of S_2N_2 ligand to two 12 valence electron metal fragments $[Mo(NO)Cl_4]^+$. The percentage of the π -interaction to the total orbital interaction

energy in $[\text{S}_2\text{N}_2(\text{Mo}(\text{NO})\text{Cl}_4)_2]^{2+}$ complex is found to be higher (10.1%) than that observed in **2Mo** (Table S2, Figure S5).^[73] Thus, if exploited wisely, the versatile ligand property of the π -electron rich S_2N_2 inorganic aromatic compounds might lead to hitherto unprecedented reactivities of transition metal complexes.

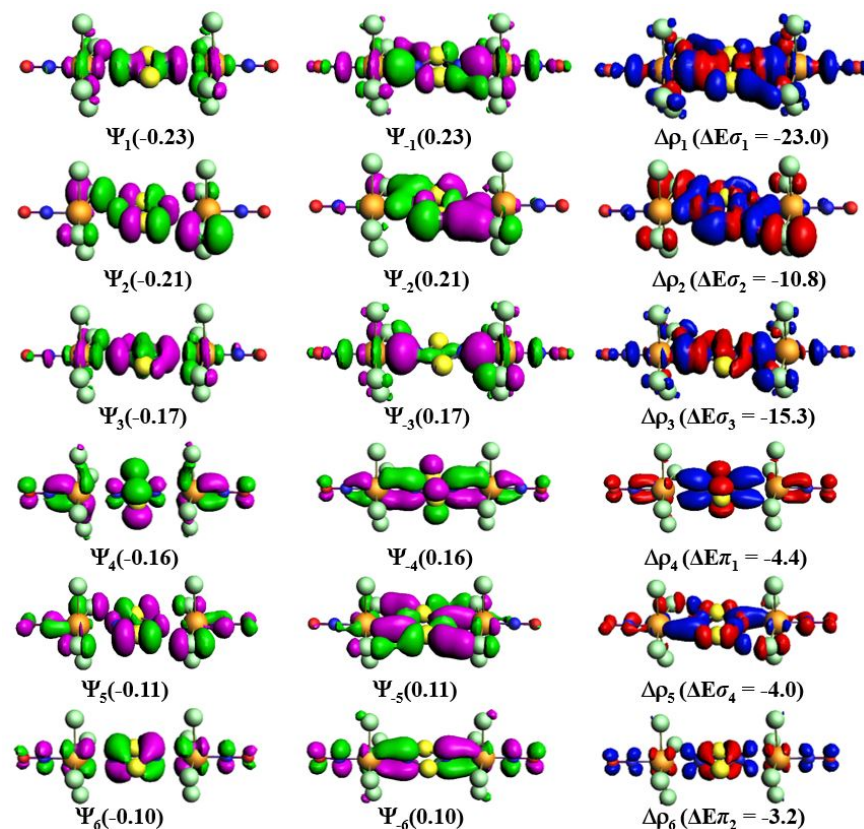


Figure 9 : Plots of NOCV pair of orbitals Ψ_{-n}/Ψ_n of pi and sigma bonding possibility in $[\text{S}_2\text{N}_2(\text{Mo}(\text{NO})\text{Cl}_4)_2]^{2-}$ with their eigen values in the parenthesis, the associated deformation densities $\Delta\rho_n$ and the orbital stabilization energies ΔE (kcal/mol) at the BP86/TZ2P/ZORA level of theory. The direction of the charge flow in the deformation density plot $\Delta\rho_n$ is from red-blue. The isosurface values for NOCV orbitals and deformation densities are 0.03 and 0.0003 respectively.

Conclusion

Electronic structure and ligand property of S_2N_2 compound towards the 14 valence electron metal fragments have been studied using quantum mechanical calculations. Our detailed theoretical calculation on S_2N_2 shows an area of charge concentration close to the direction of lone pair of N atoms of the S_2N_2 and an area of charge depletion in the extended direction of the S-N bonds of the S_2N_2 ring. In order to explore the ligand property of S_2N_2 , we have studied the complex formation of S_2N_2 with one and two square pyramidal 14 valence electron $[\text{Mo}(\text{NO})\text{Cl}_4]^-$ metal fragment(s). The molecular orbital and QTAIM analysis suggest that N-Mo σ -donation, Mo-N π -back donation, and $\text{Cl}\cdots\text{S}$ interaction through σ -hole at S-atom are present in both **1Mo** and **2Mo**. EDA-NOCV analysis has been carried out to understand the quantitative nature of bonding between $[\text{Mo}(\text{NO})\text{Cl}_4]^-$ metal fragments and S_2N_2 ligand. Our results indicate that the interaction between S_2N_2 and metal fragments has a higher electrostatic character than a covalent character. The nature of S_2N_2 as a ligand is similar in the bi-metallic complex $\text{S}_2\text{N}_2[\text{Mo}_2(\text{NO})_2(\text{Cl})_8]^{2-}$ as well. On the contrary, the σ -lone pair on N-atom in S_2N_2 is donated to the electron-deficient 12 valence electron $[\text{Mo}(\text{NO})\text{Cl}_4]^+$ fragment in $\text{S}_2\text{N}_2[\text{Mo}(\text{NO})\text{Cl}_4]^+$ and the electrons from the S_2N_2 π -MO are donated to the vacant d-orbitals of the metal

fragment. Similar bonding nature is also observed in the bi-metallic $S_2N_2[Mo_2(NO)_2(Cl)_8]^{2+}$ complex. In addition, all these complexes show donation of lone pair on Cl attached to transition metal fragment to the S-N σ^* -MO, which is majorly located on the S-atom. Here, the S-atom in S_2N_2 can be considered as a σ -hole, which is involved in the chalcogen bond with Cl-atom. Hence, our theoretical results suggest that the S_2N_2 is a versatile ligand which can be tuned as σ -donor, σ - acceptor, π -donor and π -acceptor. Thus, if exploited wisely, the versatile ligand property of the π -electron rich SN inorganic aromatic compounds might lead to hitherto unprecedented reactivities of transition metal complexes. We also analyzed the strength of the π bonding and aromaticity of S_2N_2 ring has been investigated using the EDA–NOCV analysis. EDA results indicate that S_2N_2 ligand in $S_2N_2[Mo_2(NO)_2(Cl)_8]^{2-}$ is more aromatic than S_2N_2 molecule.

Conflicts of interest

There are no conflicts of interest to declare.

Acknowledgements

SD thanks partial financial support from DST (IFA12-CH-76, CRG/2019/002891), seed grant from CUSAT for new research initiative and UGC-SAP, DST-PURSE grant at CUSAT. The computer center at CUSAT is also acknowledged for providing the computational facility set up using the DST-PURSE fund. MSNK thanks CUSAT for research fellowship.

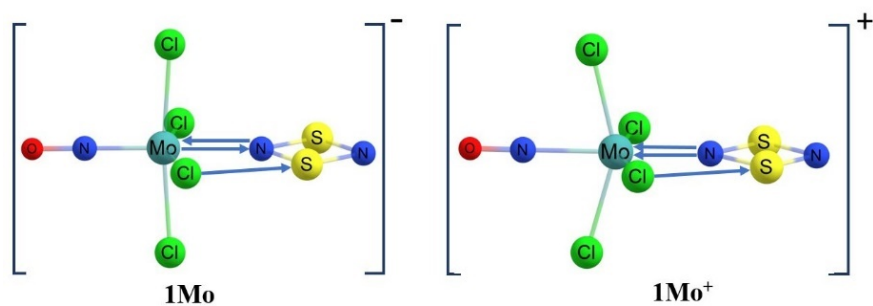
References

1. A. Togni, L. M. Venanzi, *Angew. Chem. Int. Ed. Engl.* **1994** , *33* , 497–526.
2. A. N. Khlobystov, A. J. Blake, N. R. Champness, D. A. Lemenovskii, A. G. Majouga, N. V. Zyk, M. Schroder, *Coord. Chem. Rev.* **2001** , *222* , 155–192.
3. W. Kaim, *Coord. Chem. Rev.* **2002** , *230* , 127–139.
4. M. A. Halcrow, *Coord. Chem. Rev.* **2005** , *249* , 2880–2908.
5. A. de Bettencourt-Dias, P. S. Barberb, S. Viswanathanc, *Coord. Chem. Rev.* **2014** , *273–274* , 165–200.
6. H. Nose, M. T. Rodgers, *J. Phys. Chem. A* **2014** , *118* , 8129–8140.
7. J. E. Huheey, *Inorganic Chemistry Principles of Structure and Reactivity* , 2nd ed.; Harper & Row, Publishers: New York, **1978** ; pp 403–412.
8. D. A. Estrin, O. Y. Hamra, L. Paglieri, L. D. Slep, J. A. Olabe, *Inorg. Chem.* **1996** , *35*, 6832–6837.
9. S. Pal, *Pyridine: A Useful Ligand in Transition Metal Complexes* , Ed., London: IntechOpen, **2018** . pp. 57–74.
10. L. H. Simons, P. E. Riley, R. E. Davis, J. J. Lagowski, *J. Am. Chem. Soc.* **1976** , *98* , 1044–1045.
11. A. N. Khlobystov, A. J. Blake, N. R. Champness, D. A. Lemenovskii, A. G. Majouga, N. V. Zyk, M. Schroder, *Coord. Chem. Rev.* **2001** , *222* , 155–192.
12. K. Nomiya, K. Tsuda, N. C. Kasuga, *J. Chem. Soc., Dalton Trans.* **1998** , 1653–1659.
13. K. Nomiya, K. Tsuda, Y. Tanabe, H. Nagano, *J. Inorg. Biochem.* **1998** , *69* , 9–14.
14. K. Nomiya, K. Tsuda, T. Sudoh, M. Oda, *J. Inorg. Biochem.* **1997** , *68* , 39–44.
15. K. Nomiya, R. Noguchi, K. Ohsawa. K. Tsuda, M. Oda, *J. Inorg. Biochem.* **2000** , *78* , 363–370.
16. F. Fache, E. Schulz, M. L. Tommasino, M. Lemaire, *Chem. Rev.* **2000** , *100* , 2159–2231.
17. T. Chivers, *A Guide to Chalcogen-Nitrogen Chemistry* ; World Scientific Publishing Co. Pte. Ltd.: Singapore, **2005** .
18. S. De, M. N. K. Sadik, S. Liya, *ChemistrySelect* **2019** , *4* , 8807–8814.
19. T. Chivers, R. S. Laitinen, *Dalton Trans.* **2020** , *49* , 6532–6547.
20. O. C. M. Davis, *J. Chem. Soc., Trans.* , **1906** , *89* , 1575–1578.
21. H. Wolbling, *Z. Anorg. Allg. Chem.* **1908** , *57* , 281–289.
22. T. Chivers, F. Edelmann, *Polyhedron* **1986** , *5* , 1661–1699.
23. K. Dehnicke, U. Muller, *Transition Met. Chem.* **1985** , *10* , 361–368.
24. I. Haiduc, *J. Coord. Chem.* **2019** , *72* , 2127–2159.
25. M. B. Hursthouse, K. M. A. Malik and S. N. Nabi, *J. Chem. Soc., Dalton Trans.* **1980** , 355–359.

26. G. Schmid, R. Greese, R. Boese, *Z. Naturforsch.* **1982** ,37B , 620–626.
27. A. D. Becke, *Phys. Rev. A* . **1988** , 38 , 3098–3100.
28. J. P. Perdew, *Phys. Rev. B* . **1986** , 33 , 8822–8824.
29. C. Chang, M. Pelissier and P. Durand, *Phys. Scr.* **1986** ,34 , 394–404.
30. J. –L. Heully, I. Lindgren, E. Lindroth, S. Lundquist, A. –M. M. Pendrill, *J. Phys. B* **1986** , 19 , 2799–2815.
31. E. v. Lenthe, E. J. Baerends, J. G. Snijders, *J. Chem. Phys.***1993** , 99 , 4597–4610.
32. E. v. Lenthe, J. G. Snijders, E. J. Baerends, *J. Chem. Phys.***1996** , 105 , 6505–6516.
33. E. v. Lenthe, R. v. Leeuwen, E. J. Baerends, J. G. Snijders,*Int. J. Quantum Chem.* . **1996** , 57 , 281–293.
34. E. v. Lenthe, E. J. Baerends, *J. Comput. Chem.***2003** , 24 , 1142–1156.
35. E. J. Baerends, T. Ziegler, A. J. Atkins, J. Autschbach, O. Baseggio, D. Bashford, A. Berces, F. M. Bickelhaupt, C. Bo, P. M. Boerrigter, ADF 2018, SCM, Program for EDA calculation, Theoretical Chemistry, Vrije Universiteit, Amsterdam (Netherlands), **2018** .
36. G. te Velde, F. M. Bickelhaupt, E. J. Baerends, C. F. Guerra, S. J. A. van Gisbergen, J. G. Snijders, T. Ziegler, *J. Comput. Chem.***2001** , 22 , 931–967.
37. A. E. Reed, L. A. Curtiss, F. Weinhold, *Chem. Rev.***1988** , 88 , 899–926.
38. Z. Chen, C. S. Wannere, C. Corminboeuf, R. Puchta, P. V. R. Schleyer, *Chem. Rev.* **2005** , 105 , 3842–3888.
39. M. J. Frisch, G. W. Trucks, H. B. Schlegel, G. E. Scuseria, M. A. Robb, J. R. Cheeseman, G. Scalmani, V. Barone, B. Mennucci, G. A. Petersson Gaussian 09, Revision D.01; Gaussian, Inc.: Wallingford, CT,**2009** .
40. T. Lu, F.-W. Chen, *J. Comput. Chem.* . **2012** , 33 , 580–592.
41. W. Humphrey, A. Dalkea, K. Schulten, *J. Mol. Graph.***1996** , 14 , 33–38.
42. R. F. W. Bader, *In Atoms in Molecules: A Quantum Theory*(Oxford: Clarendon Press) 1990.
43. R. F. W. Bader, *Acc. Chem. Res.* . **1985** , 18 , 9–15.
44. R. F. W. Bader, *Chem. Rev.* **1991** , 91 , 893–928.
45. S. J. Grabowski, *Chem. Rev.* **2011** , 111 , 2597–2625.
46. S. J. Grabowski, *J. Phys. Chem. A* **2012** , 116 , 1838–1845.
47. F. Weinhold, *J. Comput. Chem.* **2012** , 30 , 2440–2449.
48. Y. Zhao, D. G. Truhlar, *Theor. Chem. Acc.* **2008** ,120 , 215–241.
49. F. Weigend, R. Ahlrichs, *Phys. Chem. Chem. Phys.* **2005** ,7 , 3297–3305.
50. M. P. Mitoraj, A. Michalak, T. Ziegler, *J. Phys. Chem. A***2008** , 112 , 1933–1939.
51. M. P. Mitoraj, A. Michalak, T. Ziegler, *J. Chem. Theory Comput.***2009** , 5 , 962–975.
52. K. Morokuma, *J. Chem. Phys.* **1971** , 55 , 1236–1244.
53. T. Ziegler, A. Rauk, *Theor. Chim. Acta.* **1977** ,46 , 1–10.
54. A. G. MacDiarmid, C. M. Mikulski, P. J. Russo, M. S. Saran, A. F. Garito, A. J. Heeger, *J. Chem. Soc. Chem. Commun.* **1975** , 476–477.
55. C. M. Mikulski, J. Russo, M. S. Saran, A. G. MacDiarmid, A. F. Garito, A. Heeger, *J. Am. Chem. Soc.* **1975** , 97 , 6358–6363.
56. A. Perrin, A. F. Antognini, X. Zeng, H. Beckers, H. Willner, G. Rauhut, *Chem. Eur. J.* **2014** , 20 , 10323 – 10331.
57. T. M. Krygowski, M. K. Cyranski, *Chem. Rev.* **2001** ,101 , 1385–1420.
58. A. L. Allred, *J. Inorg. Nucl. Chem.* **1961** , 17 , 215–221.
59. T. Chivers, *Acc. Chem. Res.* **1984** , 17 , 166–171.
60. P. B. Karadakov, M. A. H. Al-Yassiri, D. L. Cooper, *Chem. Eur. J.* **2018** , 24, 16791–16803.
61. Y. Jung, T. Heine, P. v. R. Schleyer, M. Head-Gordon, *J. Am. Chem. Soc.* **2004** , 126, 3132–3138.
62. I. Fernandez, G. Frenking, *Faraday Discuss.* . **2007** ,135 , 403–421.
63. L. Zhao, M. v. Hopffgarten, D. M. Andrada, G. Frenking, *WIREs Comput Mol Sci.* **2018** , 8 , 1–37.
64. D. Cremer, E. Kraka, *Angew. Chem. Int. Ed. Engl.* **1984** , 23, 627–628.
65. M. Palusiak, T. M. Krygowski, *Chem. Eur. J.* **2007** ,13 , 7996–8006.

66. H. Wang, W. Wang, W. J. Jin, *Chem. Rev.* **2016** ,116 , 5072-5104.
67. B. Lu, X. Zhang, L. Meng, Y Zeng. *J. MolModel* . **2017** , DOI: 10.1007/s00894-017-3407-8.
68. M. J. S. Dewar, *Bull. Soc. Chim. Fr.* **1951** , 18, C71-C79.
69. J. Chatt, J. A. Duncanson, *J. Chem. Soc.* **1953** ,3 , 2939–2947.
70. A. Bondi, *J. Phys. Chem.* **1964** , 68 , 441–451.
71. V. Oliveira, D. Cremer, E. Kraka, *J. Phys. Chem. A* **2017** , 121 , 6845–6862.
72. L. Vogel, P. Wonner, S. M. Huber, *Angew. Chem. Int. Ed.***2018** , 58 , 1880-1891.
73. For details see Table S2 in ESI.
74. A. Frankenau, K. Dehnicke, U. Fenske, *Z. Anorg. Allg. Chem.* **1987** , 554 , 101–107.
75. A. Bencini, I. Ciofini, C. A. Daul, A. Ferretti, *J. Am. Chem. Soc.* **1999** , 121, 11418–11424.

Table of Content



Flexible ligation property : S₂N₂ is a versatile ligand which can be tuned as σ-donor, σ- acceptor, π-donor and π-acceptor depending upon the transition metal fragments.